Multiexcitons in type-II colloidal semiconductor quantum dots

Dan Oron, Miri Kazes, and Uri Banin
The Institute of Chemistry and the Center for Nanoscience and Nanotechnology, The Hebrew University of Jerusalem, Jerusalem 91904, Israel[*]

(Received 14 November 2006; published 22 January 2007)

The spectroscopy and dynamics of multiple excitations on colloidal type-II CdTe/CdSe core-shell quantum dots (QDs) are explored via quasi-cw multiexciton spectroscopy. The charge separation induced by the band offset redshifts the exciton emission and increases the radiative lifetime. In addition, we observe a significant modification of multiexciton properties compared with core-only or type-I QDs. In particular, the Auger recombination lifetimes are significantly increased, up to a nanosecond time scale. While in type-I QDs the Auger lifetime scales with the volume, we find for type-II QDs a scaling law that introduces a linear dependence also on the radiative lifetime. We observe a blueshift of the biexciton emission and extract biexciton repulsion of up to 30 meV in type-II QDs. This is assigned to the dominance of the Coulomb repulsion as the positive and negative charges become spatially separated, which overwhelms the correlation binding term. Higher electronic excited states can remain type I even when the lowest transition is already type II, resulting in a different size dependence of the triexciton emission. Finally, we discuss the possibilities of "multiexciton band gap engineering" using colloidal type-II QDs.

DOI: 10.1103/PhysRevB.75.035330 PACS number(s): 78.67.Hc

I. INTRODUCTION

Dimensionality governs the electronic structure of semiconductors allowing for band-gap-engineered materials exemplified in highly developed two-dimensional (2D) quantum wells (QWs), 1D wires, and 0D quantum dots (QDs).[1] The band alignment of the heterostructure is critical for determining its properties where either enclosed (type-I) or staggered (type-II) structures are possible. For several decades, this has provided rich grounds for basic research on optical and electronic properties as well as for the realization of important practical optoelectronic devices from these nanostructures. Multiexciton states in such systems reveal many-body interactions and are also important for optical gain applications.[2,3] In the type-II structures formed from QWs and epitaxial QDs the ability to engineer such multiexciton states is limited because of the relatively low energetic barriers.[4] Here we intend to show possibilities to control multiexciton properties in colloidally grown QDs.

The vast majority of recent studies on multiexciton states in colloidal nanocrystals[3,5–7] focused on type-I nanocrystals, where both charge carriers occupy the same volume. The dynamics of multiexciton states in these QDs is dominated by an ultrafast nonradiative decay via an Auger mechanism, with typical size-dependent relaxation times ranging from tens to hundreds of picoseconds. The Auger recombination lifetime has been shown to scale with the nanocrystal volume in these QDs for both CdSe and PbSe nanocrystals.[8,9] This scaling is in reasonable agreement with theoretical predictions,[10] although a comprehensive theory behind it is still lacking. The rapid nonradiative recombination is a major inhibiting factor in the achievement of efficient gain from colloidal-based devices. Since the electronic ground state is at least doubly degenerate, population inversion requires that some of the QD population be multiply excited. This becomes more pronounced since the doubly excited [biexciton (BX)] state is redshifted relative to the exciton (X) emission due to a net binding energy between the two electron-hole pairs.[11–13] Auger recombination could also be a significant hindrance in high-yield colloidal-based photovoltaic cells utilizing the carrier multiplication effect, where a single photon generates more than one electron-hole pair,[9,14] requiring charge separation to occur faster than dissipation by Auger recombination.

Auger relaxation times and binding energies in type-I nanocrystals are relatively robust features. The main handle on the Auger process is the QD size.[8] The BX binding, however, only weakly depends on it.[15,16,18,19] Morphology presents an alternative route to control the Auger process. Elongated quantum rods have longer Auger lifetimes, particularly for higher excited states,[20] and possess improved optical gain characteristics compared with spherical dots,[7] also due to smaller BX binding energies.[19] Composition in core-shell nanoparticles is yet another. Inverted type-I ZnSe/CdSe core-shell nanocrystals, where charge carriers are localized in the shell, show longer Auger lifetimes compared with core-only QDs, in particular in the regime where the electron is confined to the shell, while the hole is delocalized.[21] While this structure is in some aspects reminiscent of a type-II structure, it is actually an intermediate between a type-I and type-II structure. Therefore, in practice, neither of the above described methods was shown to qualitatively alter BX properties.

Here we explore the use of recently introduced colloidal type-II QDs[22] as a means to increase the degree of control over multiexcitonic properties in colloidal semiconductor nanocrystals and consider the validity of the type-I scaling of the multiexciton parameters for this system. Experimentally, we observe an increase of the Auger recombination lifetime in type-II QDs, well beyond the volume scaling of type-I QDs. Moreover, by tuning the composition we can modify the sign of the biexciton binding energy, inducing a repulsive Coulomb-dominated interaction, rather than an attractive correlation-dominated interaction between the electron-hole pairs. This is accounted for by a modified scaling for this

interaction. Due to the large energy gap between the ground state and higher excited states, we can, unlike in QWs or epitaxially grown QDs, independently control the properties of higher excited states, which can be tuned to have either type-I or type-II behavior, even when the ground state is type-II.

II. MATERIALS AND METHODS

As a model system to study multiexcitonic states in type-II QDs we chose CdTe/CdSe core-shell nanocrystals. In these QDs, the hole is confined to the CdTe core, while the electron is confined to the CdSe shell for a thickness of more than ≈1 nm. These particles were recently introduced as a means to obtain emission redshifted relative to the band gaps of either of the two constituents[22] and are appropriate for bioimaging applications due to their near-infrared (NIR) emission.[23] The particles used in our study have a 3.9-nm CdTe core, synthesized following the protocol of Ref. 24, where the Cd:Te ratio was modified to 1:1. In a single-pot approach, after preparing the cores, the core solution was cooled to 150 °C and a CdSe shell was grown on it using a 1-*M* solution of $Cd(Ac)_2 \cdot H_2O$ and Se in tributyl phosphine diluted to 0.2 *M* in octadecene.[22,25] Several aliquots, corresponding to several shell thicknesses, were used for the measurements.

We perform multiexciton experiments using the recently introduced quasi-continuous-wave (qcw) excitation method.[19] In this method, an optical excitation pulse long compared to the Auger lifetimes is used and the photon absorption rate is kept smaller than the relaxation rate to the band edge. In this manner, each absorption event is practically independent of previous ones. The number of excitons per QD is determined in this regime by a steady-state ladder climbing process, where higher multiexcitonic states are sequentially generated upon increasing the excitation fluence. The laser source used in our experiments is a frequency-doubled *Q*-switched Nd:YAG laser providing 5-ns pulses at 10 Hz. Pulses were focused, at room temperature, to an area of 5 mm^2 in a cuvette containing a low optical density (≈0.1 at the *X* peak) QD toluene solution. Fluorescence emission was collected by a 0.5 numerical aperture lens and directed through a monochromator onto a photomultiplier tube. The signal was detected on a digital oscilloscope triggered by a fast Si *p-i-n* photodiode. Transient emission spectra were obtained by scanning the monochromator wavelength over the entire emission spectral range.

Modeling of this system is performed using an effective mass model,[26] where the valence band offset is taken from Ref. 27 and the ligands are assumed to have an offset of 3 eV. Calculations were performed for both the lowest *S* and the lowest *P* states. Radiative lifetimes and Coulomb interaction energies were obtained following the procedures described in Ref. 26.

III. RESULTS AND DISCUSSION

A. Basic photophysics of the CdTe/CdSe type-II QDs

Let us first discuss the optical properties of singly excited type-II QDs. The QDs used in this study have a CdTe core with a diameter of 3.9 nm and a CdSe shell of varying thickness, up to 2.5 nm. The absorption spectra presented in Fig. 1 show, from bottom to top, the change in the absorption edge with increasing shell thickness (consecutive traces are shifted vertically for clarity). Initially a redshift of the *X* absorption is observed. The third aliquot, corresponding to a shell thickness of 0.9 nm, already shows smearing of the *X* absorption typical of a transition to type II. A transmission electron microscope (TEM) image of this aliquot is shown in the inset. Overall, the *X* emission shifts from 612 nm in the CdTe core to 830 nm for a CdSe shell thickness of 2.5 nm.

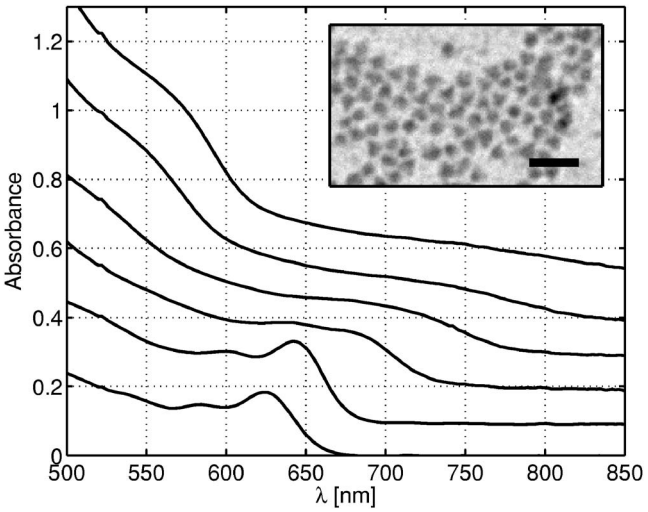

FIG. 1. Absorption spectra of colloidal CdTe/CdSe core-shell nanoparticles with a 3.9-nm core and shell thicknesses of 0.2, 0.5, 0.9, 1.5, 2.15, and 2.5 nm (total diameter 4.3, 4.9, 5.7, 6.9, 8.2, and 8.9 nm, respectively). Consecutive spectra are shifted vertically for clarity. The inset shows a TEM image of nanoparticles with a 0.9-nm shell. The bar length is 20 nm.

An effective mass calculation for the system with a shell thickness of 0.9 nm is shown in Fig. 2(a). Indeed, it shows a transition to type II; i.e., the *S*-electron wave function (dashed line) starts to localize in the CdTe core, in good agreement with the smearing of the absorption peak as shown in Fig. 1. The spatial separation of the positive and negative charges is clearly observed. Note that for this shell thickness the lowest *P*-electron state is still delocalized. Calculations indicate that it becomes localized in the shell only for a shell thickness of about 1.5 nm.

Figure 2(b) shows the measured *X* emission lifetime, which increases from 20 ns in the cores to 140 ns for a 2.5-nm shell. These values were deduced from time-resolved emission traces, which show a small instantaneous component and a single-exponential decay thereafter. The instantaneous component is attributed to QDs having a very low quantum efficiency due to nonradiative decay routes, while the exponentially decaying term is attributed to well-passivated QDs. Since the latter are typically known to have quantum efficiencies approaching unity,[28,29] we believe the measured slowly decaying component is mainly determined by radiative decay. This is corroborated by the single-exponential behavior. We also calculate, using the effective mass model, the expected increase in the radiative lifetime

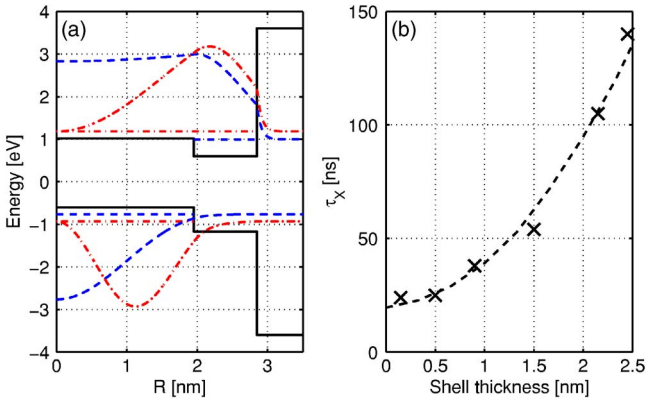

FIG. 2. (Color online) (a) Calculated radial electron (top) and hole (bottom, inverted) probability distribution functions for both the lowest S state (dashed line) and the lowest P state (dash-dotted line) for a shell thickness of 0.9 nm. For clarity, wave functions are shifted by the level energy (dashed and dash-dotted horizontal lines, respectively). (b) Measured X emission lifetime ($\times$ symbols) and the effective mass model prediction (dashed line), based on the e-h overlap integral.

by considering the change in the overlap integral $|\int dV \psi_e \psi_h|^2$ as a function of shell thickness. This is shown as a dashed line in Fig. 2(b) and is in very good agreement with the measured lifetime, further supporting the attribution of the measured lifetime to a radiative process. Note that despite the inaccuracy of the effective mass model in describing the valence band, it should model quite accurately the overlap term, since the overlap between the S-electron and hole wave functions is mostly determined by the penetration of the electron wave function into the core. The hole wave function decreases rapidly in the shell due to both the higher effective mass and the larger valence band offset.

B. Scaling of the multiexciton Auger recombination lifetime in type-II QDs

The dramatic effect of the transition to type II on the radiative lifetime is expected to affect not just the linear properties of QDs but also the Auger recombination process. We now proceed to measure Auger recombination rates in order to quantify this effect. Clearly, Auger recombination lifetimes cannot be directly extracted from qcw measurements, as all relevant lifetimes are significantly shorter than the excitation pulse duration. We therefore measure the effect of the photon absorption rate on the emission transients, from which one can indirectly extract the Auger recombination rate. To differentiate between the BX emission and the X emission, we take advantage of the fact that the BX emission is instantaneous, whereas the X emission is delayed. For an excitation fluence well above one photon per dot, all QDs will be at least singly excited, so that the emission immediately after the excitation pulse should be proportional to the QD density N, divided by the exciton radiative lifetime, $I_{delayed}=N/\tau_X^{rad}$. During the excitation pulse, however, there are two components to the emission: $I_{inst}=N_X/\tau_X^{rad}+N_{BX}/\tau_{BX}^{rad}$. Due to the higher number of carriers, τ_{BX}^{rad} is shorter than τ_X^{rad}. At intermediate fluences, such that triexcitons (TX) are still not excited, $N_X+N_{BX}=N$ so that the total instantaneous emission is proportional to

$$I_{inst} \propto I_{delayed}\left[1+\frac{N_{BX}}{N}\left(\frac{\tau_X^{rad}-\tau_{BX}^{rad}}{\tau_{BX}^{rad}}\right)\right]. \quad (1)$$

Thus, the instantaneous emission contains a component whose intensity is linearly dependent on the mean value of N_{BX}/N. Here we assume that the ratio of the radiative lifetimes of the X and BX is independent of the shell thickness. From available data on CdSe QDs, $\tau_X^{rad}\approx 2\tau_{BX}^{rad}$,[16,17] so that the coefficient of proportionality in Eq. (1) is in fact very close to unity. Since in this regime the mean fraction of BX is simply the photon absorption rate multiplied by the Auger recombination lifetime, $N_{BX}/N=\tau_{Auger}^{BX}(N_{ph}/t_{pulse})$ (where t_{pulse} is the excitation pulse duration and N_{ph} is the average number of photons absorbed per dot during the excitation pulse), τ_{Auger}^{BX} can (up to a constant of order unity) be extracted from

$$\tau_{Auger}^{BX}=t_{pulse}\left.\frac{d(I_{inst}/I_{delayed})}{dN_{ph}}\right|_{N_{ph}=0}. \quad (2)$$

Turning to the experimental results, we show a typical measured time trace, measured for QDs with a 0.9-nm shell at the X emission peak (700 nm) and at a pulse energy of 600 μJ in Fig. 3(a). This trace is decomposed into an instantaneous component (dashed line) and a slowly decaying one (dash-dotted line), corresponding to a single exponential. This is done by a least-squares fit over the two relative amplitudes and an overall time delay (which is typically less than 0.5 ns, due to timing jitter of the triggering) using the measured detector response for the instantaneous component and its convolution with the measured X lifetime for the slowly decaying one. In this case, the transient component is predominantly due to emission from multiexcitonic states, but contains a contribution from the X saturation and from QDs with short (i.e., a few nanoseconds) lifetimes.

To obtain Auger lifetimes, we require exact knowledge of the photon absorption rates. To translate the pulse energy to an average number of photons per dot we measure the saturation of the delayed emission component as a function of pulse energy, as shown in Fig. 3(b). The integrated intensity in a time window of 5–75 ns after the excitation pulse is then fitted to a curve of the form $A[1-\exp(E/E_1)]$, where E_1 is the energy required for an average of one photon per dot, denoted by the vertical black line (25 μJ in this case). Using this we now plot the ratio $R=I_{inst}/I_{delayed}$ as a function of the number of absorbed photons per dot [Fig. 3(c)]. We initially observe a linear increase of the transient BX population. When the photon absorption rate equals the BX Auger recombination rate (i.e., $t_{pulse}/N_{ph}=\tau_{BX}^{Auger}$, where t_{pulse} is the excitation pulse duration) the BX population saturates and higher multiexcitonic states are observed. This saturation is observed as a slower increase in R and indicates state filling of the BX and excitation of TX. As discussed above, the derivative at $N=0$ is proportional to the Auger recombination lifetime.

Note that the above analysis is applicable as long as $\tau_{Auger}^{BX}\ll t_{pulse}$, so that the Poissonian distribution of the num-

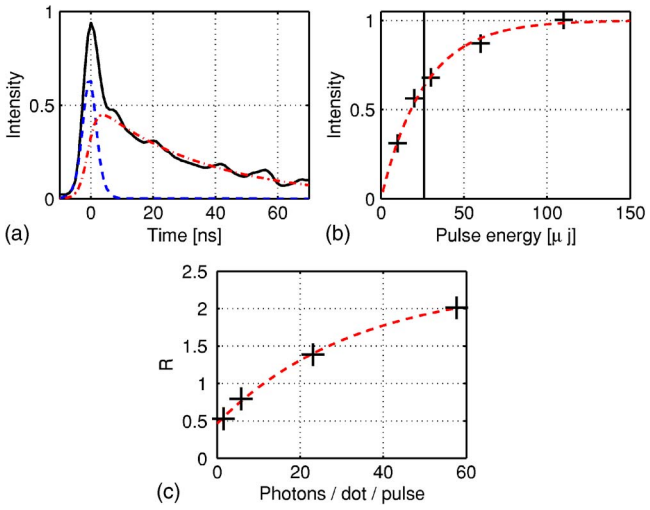

FIG. 3. (Color online) Methods for extraction of the Auger recombination lifetime, demonstrated on 3.9-nm CdTe core, 0.9-nm-thick CdSe shell nanoparticles. (a) Emission transient measured at the X peak (700 nm) at a 600 μJ pulse energy (solid line) and its decomposition into an instantaneous component (dashed line) and a slowly decaying (35-ns) component (dash-dotted line). (b) Translation of pulse energies to average number of absorbed photons by fitting the integrated delayed emission intensity (from 5 ns after the excitation pulse to 75 ns, plus signs) to a saturation curve (dashed line). The vertical line at $\approx$25 μJ indicates the energy for absorption of one photon per dot. According to this, the curve shown in (a) corresponds to about 25 absorbed photons per dot. (c) The measured ratio of the instantaneous component and the slowly decaying one as a function of the number of absorbed photons per dot (plus signs) along with a saturation curve (dashed line).

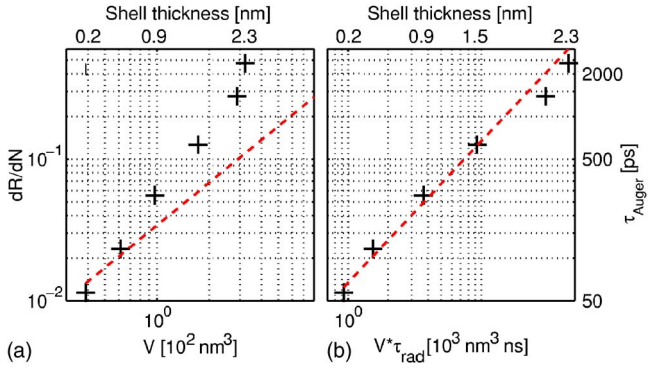

FIG. 4. (Color online) The derivative of the measured ratio of the instantaneous component and the slowly decaying one with respect to the absorbed number of photons (left axis) and a corresponding approximate BX Auger lifetime (right axis) as a function of (a) QD volume (dashed line is a linear dependence, corresponding to the type-I scaling) and (b) $V\tau_{rad}$. This fits very well with a linear dependence (dashed line).

ber of absorbed photons per dot is narrow. When τ_{Auger}^{BX} becomes comparable to the pulse duration this underestimates the BX Auger relaxation time due to a contribution of the more rapidly decaying TX to the emission transient even at low intensities.

The Auger lifetimes extracted by this method for all shell thicknesses are shown as a function of QD volume in Fig. 4(a). Note that our results for the 3.9-nm CdTe core agree well with time-resolved measurements of the Auger rate for CdSe QDs of a similar size.[8] Overall, we find that the Auger lifetime increases much faster than the QD volume, significantly deviating from a linear dependence (dashed line). This is in contrast to experimental observations on type-I QDs (Ref. 8) and the prediction by Ivanov *et al.*[21] for type-II dots.

We now look for a modification of the type-I scaling law $\tau_{Auger} \propto V$ which will take into account the effects of charge separation. We believe that the simple volume scaling fails in type-II QDs since it does not take into account the reduced overlap between the electron and hole wave functions. Intuitively, we can break the Auger process into two parts: a recombination event and an energy transfer event. It is obvious that the probability of the recombination event should be dramatically affected by the transition to type II. Since this effect is also accounted for in the single-exciton radiative lifetime, we propose a modified scaling $\tau_{Auger} \propto V\tau_{rad}$, which takes into account the reduction in the recombination probability due to the charge separation. Note that this is a generalization of the type-I volume scaling, since in type-I QDs the radiative lifetime only weakly depends on size.[30] As can be seen in Fig. 4(b), a linear dependence (dashed line) on $V\tau_{rad}$ [where τ_{rad} is approximated by the measured long X decay component of Fig. 3(b)] fits well with the measured data. As expected for the samples with a thicker shell, where the Auger lifetime approaches the pulse duration and, hence, the procedure for extraction of the Auger lifetime becomes less valid, the data points lie below the linear curve. Overall, we observe Auger recombination lifetimes of the order of 1 ns, significantly longer than those observed in any colloidal system of similar size.

C. Multiexciton spectral shifts in type-II QDs

We now turn to observe the measured multiexciton emission spectra. It has been suggested that in type-II QDs the energy shift of the BX relative to the X, Δ_{XX}, might change its sign from negative (binding) to positive (repulsion).[21,31] This was also predicted[32] for epitaxially grown type-II QDs and observed in epitaxially grown pyramidal Ge/Si QDs.[33] The reason for this transition to repulsion is twofold: the decrease in correlation energy as compared with type-I QDs due to charge separation and the increase of the repulsive perturbative contribution to the Δ_{XX} due to the Coulomb interaction of fixed single-particle orbitals.[34]

Multiexciton emission spectral locations are extracted by fitting several transient emission spectra, measured at the peak of the excitation pulse at several excitation energies. Two examples of such series of spectra, at energies varying from 40 μJ to 6 mJ per pulse, are shown in Figs. 5(a) and 5(b). Briefly, the X emission is obtained from the lowest-energy data, where $\approx$1 photon is absorbed per dot. The set of spectra measured at higher illumination intensities is fitted using two additional peaks (each with an arbitrary spectral location and spectral width), accounting for BX and TX emission. In Fig. 5(a) we plot spectra obtained for QDs with a 0.9-nm shell. Little change is observed up to the highest energies despite the significant multiexciton emission at

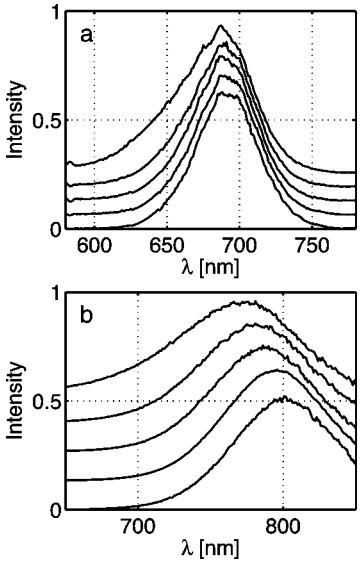

FIG. 5. Transient spectra measured at the peak of the excitation pulse at increasing pulse energies (40, 150, 600, 1500, and 6000 μJ) for (a) QDs with a 0.9-nm CdSe shell, just at the transition from type I to type II. No shift is observed in the first few spectra, corresponding to nearly zero BX shift. (b) QDs with a 2.15-nm CdSe shell, already in the type-II regime. The blueshift indicates a repulsive BX state.

higher energies. This is since the BX emission practically lies on top of the X emission, already showing deviation from type-I behavior, where a redshifted BX emission (with a binding energy of the order of 30 meV) is observed. The blueshifted shoulder appearing at the highest intensities is due to the TX emission. In Fig. 5(b) we plot spectra obtained for QDs with a 2.15-nm shell. In this case, a clear blueshift is observed as soon as multiexciton states are generated. In general, the fit results can vary by up to 2 nm depending on the exact details of the fitting procedure (particularly the choice of energies of the spectra used), corresponding to a maximal error of about 6 meV. The error may be somewhat larger for the largest type-II dots, where, due to the redshifted emission, the detector responsivity falls significantly. A detailed description of the fitting procedure appears elsewhere.[19]

The measured Δ_{XX} extracted from the qcw spectra (denoted by plus signs) is plotted in Fig. 6(a) as a function of the shell thickness. We observe a transition to repulsion at the same shell thickness where the exciton peak is smeared in the absorption spectrum of Fig. 1(a) and in good agreement with the prediction of the effective mass model for this transition. The maximal blueshift we observe is $\approx$30 meV. To model this effect, we consider the two extremities limiting Δ_{XX}. The dashed line is a numerical approximation to the measured Δ_{XX} ($\times$ symbols) in CdSe QDs of a similar diameter. The dash-dotted line shows the Coulomb repulsion as calculated from the effective mass model assuming fixed single-particle wave functions. The solid line is a weighted average between the two:

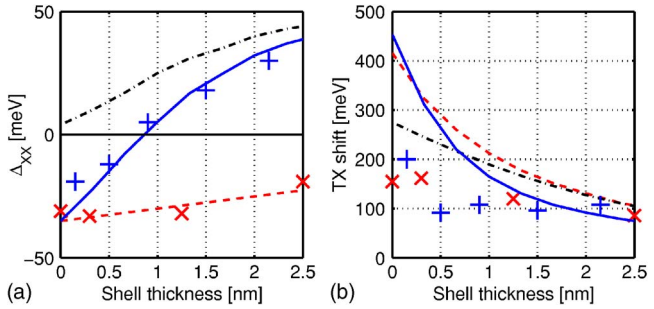

FIG. 6. (Color online) Multiexciton shifts as a function of shell thickness. (a) Measured Δ_{XX} in CdTe/CdSe QDs (plus signs) and in CdSe QDs of similar diameter ($\times$ symbols). While type-I QDs (CdSe) show binding; upon transition to type II a shift to repulsion is observed. A theoretical prediction (solid line) for the type-II QDs based on a weighted average between the measured binding energy of type-I QDs (dashed line) and the model prediction for the repulsion energy (dash-dotted line) are also shown. (b) Measured TX shift in CdTe/CdSe QDs (plus signs) and in CdSe QDs of similar diameter ($\times$ symbols), compared with the calculated $1P_e$ to $1S_e$ shift (solid line and dashed line, respectively). The measured $1P$ to $1S$ shift for CdSe QDs (extrapolated from Ref. 35) is shown as a dash-dotted black line.

$$\Delta_{XX} = \Delta_{XX}^{binding} \int_{core} dV|\psi_e|^2 + \Delta_{XX}^{repulsive} \int_{shell} dV|\psi_e|^2, \quad (3)$$

where ψ_e is taken from the model, showing excellent agreement with measurements.

We also examine the binding energies of higher multiexcitonic states. In Fig. 6(b) the measured TX energy shifts are compared with the calculated energy separation between the $1S_e$ and $1P_e$ states in the single exciton regime. We compare the results for CdSe QDs with those obtained for CdTe/CdSe QDs. For the CdSe QDs we also plot the measured shift as obtained from photoluminescence excitation experiments.[35] As can be seen, the model overestimates the shift for small dots but reproduces it quite well for larger ones, which is, in our case, the region of interest. For the CdSe QDs the measured TX emission ($\times$ symbols) is always redshifted with respect to both the experimental and model predictions (dash-dotted line and dashed line, respectively), indicating binding of the TX. The TX shift decreases with QD size. For the CdTe/CdSe QDs we see that the measured TX shift (plus signs) is practically independent of the shell thickness for shells thicker than about 0.5 nm. For the largest CdTe/CdSe QDs, the observed shift appears slightly larger than in CdSe QDs of equal size, despite the fact that the effective mass model predicts a smaller shift. The observed shift rises above the model predictions (solid line) for a shell thickness of 2.15 nm, indicating a transition to TX repulsion of the order of 20 meV. Indeed, this transition occurs at roughly a shell thickness of 1.5 nm, at which the $1P_e$ state becomes localized in the shell in the effective mass model calculation.

IV. CONCLUSIONS

The long Auger lifetimes observed in type-II QDs should facilitate achievement of prolonged optical gain in colloidal

systems. We have shown a mechanism by which the Auger recombination process can be significantly slowed down. This comes, however, at a cost of reducing the oscillator strength of the transition. The optimal trade-off between these two effects is dependent on the gain settings. Broadly speaking, lasing from QDs with larger Auger lifetimes can be achieved by raising the cavity quality factors. The reduced Auger recombination can also mitigate thermal effects due to Auger heating of the gain medium.

Following the newly discovered scaling $\tau_{Auger} \propto V\tau_{rad}$, we expect type-II structures with a larger conduction band offset, such as ZnTe/CdSe QDs, should have even longer Auger lifetimes. We also expect a larger biexciton blueshift in this system due to both the tighter confinement of the electrons and due to the reduced dielectric constant of ZnTe. While it should be possible to further increase Auger lifetimes in this material system, we see no practical utility in increasing Auger lifetimes beyond several nanoseconds, where other nonradiative decay channels may become significant. In general, varying material composition, sizes, and shapes should enable a high degree of controllability over the multiexciton optical properties of such type-II structures.

A positive value of Δ_{XX} may also open a route towards achievement of optical gain in the single-exciton regime.[21] In an inhomogeneously broadened ensemble where $\Delta_{XX}<0$ absorption by the redshifted BX state inhibits gain for all frequencies (setting the inversion threshold at exactly one exciton per dot). In contrast, in a system where $\Delta_{XX}>0$, no BX absorption inhibits the gain for the reddest QDs in the ensemble, setting the inversion threshold at less than one exciton per dot. In practice, there are several limitations towards the achievement of gain in this regime. For the particles presently used, the BX blueshift, of up to 30 meV, is relatively small compared with the emission full width at half maximum (FWHM) of about 170 meV. Moreover, gain in the single-exciton regime requires high quantum yields, more than the 20% yield reported for CdTe/CdSe/ZnTe QDs.[22]

In conclusion, we have shown that the properties of multiexciton states in type-II nanocrystals differ from those in their type-I counterparts and may differ in many aspects from type-II QW's and epitaxially grown QDs. From a practical point of view, the increased Auger lifetime and the blueshifted multiexciton emission in type-II QDs could improve the performance of optically pumped gain devices. In cases where carrier multiplication could be harnessed for photovoltaics, leading to the creation of multiexciton states, the large Auger lifetime of the type-II system could also be beneficial. Fundamentally, they can aid in elucidating the role of electron-hole interaction[36] in the ultrafast dynamics of relaxation of charge carriers to the band edge by utilizing the reduced overlap of the electron and the hole. Overall, type-II QDs offer a rich testbed for theoretical modeling of multiparticle interactions in QDs.

ACKNOWLEDGMENTS

Financial support from the Israel Science Foundation (Grant No. 924/04) and from the German-Israeli program (DIP) is gratefully acknowledged. M.K. acknowledges funding by the Israel Ministry of Science and Technology via the Eshkol scholarship program.

*URL: http://chem.ch.huji.ac.il/~nano/

[1] *Optical Properties of Semiconductor Nanostructures*, edited by M. L. Sadowski (Springer, Berlin, 2000).

[2] J. R. Meyer, C. A. Hoffman, F. J. Bartoli, and L. R. Ram-Mohan, Appl. Phys. Lett. **67**, 757 (1995).

[3] V. I. Klimov, A. A. Mikhailovsky, Su Xu, A. Malko, J. A. Hollingsworth, C. A. Leatherdale, H.-J. Eisler, and M. G. Bawendi, Science **290**, 314 (2000).

[4] E. Dekel, D. Gershoni, E. Ehrenfreund, D. Spektor, J. M. Garcia, and P. M. Petroff, Phys. Rev. Lett. **80**, 4991 (1998).

[5] A. I. Ekimov, F. Hache, M. C. Schanne-Klein, D. Ricard, C. Flytzanis, I. A. Kudryavtsev, T. V. Yazeva, A. V. Rodina, and Al. L. Efros, J. Opt. Soc. Am. B **10**, 100 (1993).

[6] H. Htoon, J. A. Hollingsworth, A. V. Malkom, R. Dickerson, and V. I. Klimov, Appl. Phys. Lett. **82**, 4776 (2003).

[7] M. Kazes, D. Y. Lewis, Y. Ebenstein, T. Mokari, and U. Banin, Adv. Mater. (Weinheim, Ger.) **14**, 317 (2002).

[8] V. I. Klimov, A. A. Mikhailovsky, D. W. McBranch, C. A. Leatherdale, and M. G. Bawendi, Science **287**, 1011 (2000).

[9] R. D. Schaller and V. I. Klimov, Phys. Rev. Lett. **92**, 186601 (2004).

[10] Al. L. Efros, in *Semiconductor Nanocrystals: From Basic Principles to Applications*, edited by Al. L. Efros, D. J. Lockwood, and L. Tsybeskov (Kluwer Academic, New York, 2003), pp. 52–72.

[11] V. I. Klimov, S. Hunsche, and H. Kurz, Phys. Rev. B **50**, 8110 (1994).

[12] B. Patton, W. Langbein, and U. Woggon, Phys. Rev. B **68**, 125316 (2003).

[13] U. Woggon, in *Optical Properties of Semiconductors and their Nanostructures*, edited by H. Kalt and M. Hetterich (Springer-Verlag, Berlin, 2004), pp. 107–129.

[14] A. J. Nozik, Physica E (Amsterdam) **14**, 115 (2002).

[15] C. Bonati, M. B. Mohamed, D. Tonti, G. Zgrablic, S. Haacke, F. van Mourik, and M. Chergui, Phys. Rev. B **71**, 205317 (2005).

[16] B. Fisher, J.-M. Caruge, Y.-T. Chan, J. Halpert, and M. Bawendi, Chem. Phys. **318**, 71 (2005).

[17] I. A. Akimov, J. T. Andrews, and F. Henneberger, Phys. Rev. Lett. **96**, 067401 (2006).

[18] M. Achermann, J. A. Hollingsworth, and V. I. Klimov, Phys. Rev. B **68**, 245302 (2003).

[19] D. Oron, M. Kazes, I. Shweky, and U. Banin, Phys. Rev. B **74**, 115333 (2006).

[20] H. Htoon, J. A. Hollingsworth, R. Dickerson, and V. I. Klimov, Phys. Rev. Lett. **91**, 227401 (2003).

[21] Sergei A. Ivanov, J. Nanda, A. Piryatinski, M. Achermann, L. P. Balet, I. V. Bezel, P. O. Anikeeva, S. Tretiak, and V. I. Klimov, J. Phys. Chem. B **108**, 10625 (2004); J. Nanda, S. A. Ivanov, H.

Htoon, I. Bezel, A. Piryatinski, S. Tretyak, and V. I. Klimov, J. Appl. Phys. **99**, 034309 (2006).
[22] S. Kim, B. Fisher, H.-J. Eisler, and M. Bawendi, J. Am. Chem. Soc. **125**, 11466 (2003).
[23] S. Kim, Y. T. Lim, E. G. Soltesz, A. M. De Grand, J. Lee, A. Nakayama, J. A. Parker, T. Mihaljevic, R. G. Laurence, D. M. Dor, L. H. Cohn, M. G. Bawendi, and J. V. Frangioni, Nat. Biotechnol. **22**, 93 (2004).
[24] W. W. Wu, L. Qu, W. Guo, and X. Peng, Chem. Mater. **15**, 2854 (2003).
[25] As shell growth proceeded the injection temperature was increased to 190 °C.
[26] J. W. Haus, H. S. Zhou, I. Honma, and H. Komiyama, Phys. Rev. B **47**, 1359 (1993); D. Schooss, A. Mews, A. Eychmuller, and H. Weller, *ibid.* **49**, 17072 (1994).
[27] S-H. Wei and A. Zunger, Appl. Phys. Lett. **72**, 2011 (1998).
[28] Y. Ebenstein, T. Mokari, and U. Banin, Appl. Phys. Lett. **80**, 4033 (2002).
[29] X. Brokmann, L. Coolen, M. Dahan, and J. P. Hermier, Phys. Rev. Lett. **93**, 107403 (2004).
[30] A. F. van Driel, G. Allan, C. Delerue, P. Lodahl, W. L. Vos, and D. Vanmaekelbergh, Phys. Rev. Lett. **95**, 236804 (2005).
[31] Al. L. Efros and A. V. Rodina, Solid State Commun. **72**, 645 (1989).
[32] Ph. Lelong, K. Suzuki, G. Bastard, H. Sakaki, and Y. Arakawa, Physica E (Amsterdam) **7**, 393 (2000).
[33] A. I. Yakimov, N. P. Stepina, A. V. Dvurechenskii, A. I. Nikiforov, and A. V. Nenashev, Phys. Rev. B **63**, 045312 (2001).
[34] J. Shumway, A. Franceschetti, and A. Zunger, Phys. Rev. B **63**, 155316 (2001).
[35] D. J. Norris and M. G. Bawendi, Phys. Rev. B **53**, 16338 (1996).
[36] E. Hendry, M. Koeberg, F. Wang, H. Zhang, C. de Mello Donega, D. Vanmaekelbergh, and M. Bonn, Phys. Rev. Lett. **96**, 057408 (2006).